Available online at www.CivileJournal.org

Civil Engineering Journal

(E-ISSN: 2476-3055; ISSN: 2676-6957)

Vol. 11, No. 08, August, 2025

The Use of Electronic Initiation Systems for Wall Control Blasting at an Open Pit Mine

Nurbol Bakhtybayev [1], Oraz Abil [1*], Asel Bakhtybayeva [1]

[1] *Mining Research Group LLP, Karaganda, 100022, Kazakhstan.*

Received 19 March 2025; Revised 22 June 2025; Accepted 04 July 2025; Published 01 August 2025

Abstract

This study investigates the effectiveness of electronic initiation systems (EIS) for wall control blasting in open-pit mining, with a specific focus on their influence on ground vibrations and rock fragmentation. The primary objective of the study is to evaluate whether EIS can achieve comparable or superior results in fragmentation quality while reducing seismic impact compared to non-electric initiation systems (NEIS). Experiments were conducted at an open-pit gold mine. During the experiments, EIS and NEIS were used. There was assessed seismicity of each blast during the experiments. Peak Particle Velocity (PPV) was measured at multiple points near the pit benches, and fragmentation of the blasted rock mass was analyzed through visual inspection and image analysis techniques. A statistical evaluation of the collected data revealed that EIS provided similar fragmentation outcomes while significantly reducing PPV values. Due to the ability to precisely time blasts and allow for optimized delay sequences and energy distribution, EIS can reduce blast vibrations. These findings suggest that EIS is a viable and efficient solution for wall control blasting, particularly in cases where pre-splitting or other conventional techniques cannot be applied due to geological or operational conditions. In this study, for the first time,the PPV was measured at the closest distance (6.57 m to the blasted block). The authors tried to find out the combination of two controversial outcomes of blasting work, rock fragmentation and ground vibrations, in this study.

Keywords: Electronic Initiation Systems; Wall Control Blasting; Peak Particle Velocity; Seismicity; Fragmentation; Powder Factor.

1. Introduction

Rock blasting is an essential and valuable process in surface mining. However, blasting often generates adverse side effects such as flyrock, air overpressure, and ground vibrations. The ground vibrations are the most critical in terms of slope stability. Excessive blast-induced ground vibrations can cause structural damage to slopes, benches, and nearby facilities. Therefore, ground vibration control becomes a vital procedure of sustainable mining practices. The Peak Particle Velocity (PPV) parameter is widely used to evaluate and monitor ground vibrations. Classical empirical models, such as the USBM equation, predict PPV based on the maximum charge per delay (MCD) and the distance between the blast and the monitoring point. While these models provide a basic estimation framework, they often overlook the influence of blast design variables, charge distribution, delay patterns, and rock mass conditions [1]. In recent years, multiple efforts have been made to enhance PPV prediction accuracy by including additional blast design parameters. Appani et al. [1] developed a multivariate regression equation incorporating parameters such as hole length, charge length, stemming, and number of holes. The model proposed by Appani et al. [1] demonstrated improved accuracy (R^2 = 0.82) compared to traditional two-variable models. Similarly, machine learning techniques, including support vector regression, random forests, and neural networks, have been adopted to model blast vibrations more effectively [2].

* Corresponding author: orazabil@minrg.com

http://dx.doi.org/10.28991/CEJ-2025-011-08-010

The reliability and timing precision of initiation systems also play a crucial role in controlling blast-induced vibrations. Electronic initiation systems (EIS) offer millisecond-level timing accuracy, reducing delay scatter and enabling better control of the energy release sequence [3]. However, Leng et al. [3] highlighted that EIS units are susceptible to impact-induced failures, necessitating robust design and quality control for consistent performance under dynamic loading. Beyond vibration control, several studies have explored the relationship between blast parameters and rock fragmentation. For instance, Hong et al. [4] demonstrated that water-deck charges improve fragmentation efficiency and reduce average fragment size. Tosun [5] proposed an empirical model to estimate the mean fragment size (X_{50}) using drilling rate and specific charge factor.

Additionally, the coupling medium (air, water, etc.) in boreholes has been shown to influence vibration characteristics. Li et al. [6] found that water-filled boreholes produce higher-energy seismic waves with lower-frequency components, which propagate farther and pose greater risk to structural stability. These findings emphasize the necessity of accounting for coupling conditions in blast design. A comprehensive perspective on blasting performance is offered by Shehu & Hashim [7], who proposed a framework that integrates technical, environmental, and operational metrics—such as fragmentation, airblast, flyrock, and PPV—into a unified efficiency assessment model. While numerical tools like FLAC3D allow for detailed simulation of stress wave propagation [8], practical decision-making in the field still heavily relies on empirical analysis and vibration monitoring.

In this context, the present study investigates the effect of various delay timing configurations using electronic initiation systems on ground vibration and rock fragmentation. Field data from gold quarry operations are analyzed to determine optimal timing strategies that minimize PPV while ensuring efficient fragmentation. The outcomes aim to support the development of safer and more effective blasting practices. With the increasing depth of open pit mines, ensuring the stability of long-term slopes and benches has become crucial. Consequently, there has been a significant increase in the requirements for preserving the pit slopes and benches. This has led to the development and widespread implementation of different types of wall control blasting, such as contour blasting, buffer blasting, presplit blasting, etc. [9].

Generally, counter blasting is used as a main wall control blasting method at the discussed mine. This method involves creating a severed slot along the benches by blasting a series of boreholes. This slot absorbs blast energy, preventing the formation of blockages and cracks [9]. There is a limitation of using the counter blasting in soft rocks and soils. According to the geomechanical requirements, the angle of slopes in weathered rocks and soils can be less than 300. In this case the counterbore hole's inclination angle should be the same as the slope inclination. Due to the high degree of rock fracturing and hydrogeology in weak rocks and soils, drilling boreholes with 30-degree inclinations is difficult or impossible because of their collapsing. The electronically initiated systems can be used as a wall control blasting solution. The article discussed results of the site experiments with replacing presplit blasting by low seismic impact technologies by using electronic initiation systems.

There are many studies that describe the level of rock mass damage depending on the measured peak particle velocity (PPV). The degrees of influence of ground displacement velocities on the rock mass have been established in studies [10–17] (see Table 1).

Table 1. Ground displacement velocities on the rock mass

Author	The Results Obtained
Bauer & Calder (1970) [10]	They observed that at a PPV of 254 mm/s, cracks in undamaged rock will not occur; a PPV of 254–635 mm/s leads to minor tensile cracking, while a PPV of 635–2540 mm/s causes significant stretching and some radial cracking. Massif destruction will occur at a velocity of 2540 mm/s.
Oriard (1982) [11]	Oriard (1982) [11] hypothesized that a significant portion of the rock massif is damaged when the PPV exceeds 635 mm/s.
Holmberg & Persson (1979) [12]	They proposed a model for estimating PPV in the near field by integrating the generalized PPV predictor equation for the total charge length. They found that the PPV level during rock damage ranges from 700 to 1000 mm/s.
Rustan et al. (1985) [13]	Rustan et al. (1985) [13] measured vibration from contour blasts with a low porosity tube charge. PPV at the minimum measured distance ranged from 300 to 900 mm/s for explosives commonly used in smooth blasting. Extrapolation to a range of 0.5 m gives a PPV of approximately 1000–3000 mm/s. This is significantly higher than the frequently mentioned damage range of 700–1000 mm/s. Calculating from 700 mm/s extends to a range of 0.1 m. The observed range of damage by direct methods is 0.5 m. This study assumes that PPV for damage may exceed 700–1000 mm/s.
Meyer & Dunn (1995) [14]	Meyer & Dunn (1995) [14] studied vibrations from blasts at the Perseverance nickel mine in Australia. A damage threshold PPV value of 600 mm/s was determined for the rock mass of the Perseverance Mine, with minor damage occurring above 300 mm/s.
Murthy et al. (2002) [15]	Murthy et al. (2002) [15] suggested that the threshold level of PPV for fracturing dense basaltic rock is 2050 mm/s.
Dey K. (2004) [16]	The modeled near-field ground vibration and the threshold PPV levels for damage onset vary within the range of 700–1300 mm/s across five horizontal tracks of metallurgical mines.

According to most researchers, the peak particle velocity (PPV) is a function of the scaled distance, which relates the distance to the blast to the explosive charge per delay interval [13].

$$PPV=K(SD)^{-B} \quad (1)$$

According to the research by Bauer & Calder (1970) [10], rock mass destruction occurs at ground displacement velocities exceeding 2540 mm/s. According to Bogdanhoff's research [18], ground displacements ranging from 2000 to 2400 mm/s were recorded at a distance of 1 m from the drilling and blasting site. Oriard (1982) [11] suggested that a significant portion of the rock massif is damaged at PPV levels above 635 mm/s [11].

2. Research Methodology

The main indicator characterizing the degree of explosion impact on the rock mass is the ground displacement velocity and acceleration. Figure 1, shows the flowchart of the research methodology through which the objectives of this study were achieved.

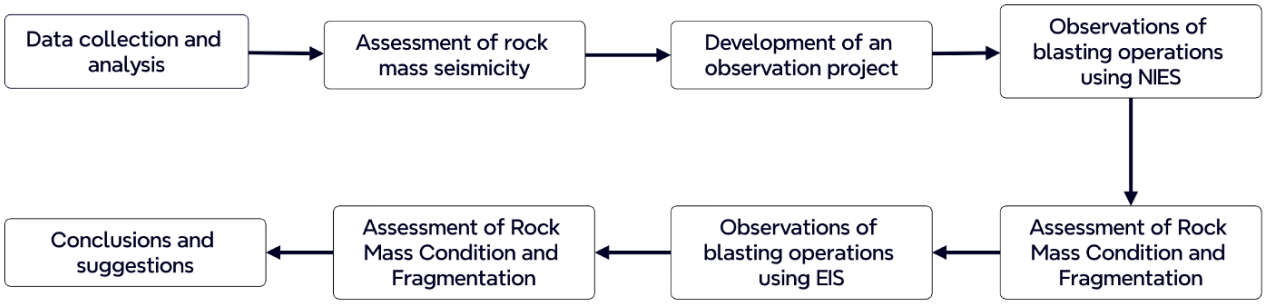

Figure 1. Workflow of the Experimental Methodology

To describe the response of different types of rock mass to the seismic impact of blasts professor Sadovsky & Kostyuchenko [19] suggested the term "rock mass seismicity". According to the Sadovsky & Kostyuchenko [19] the rock mass seismicity can be calculated by the Equation 2:

$$k_s = 0.13 \cdot f^{0.395} \cdot [(1-\eta) \cdot U_{se}]^{0.25} \quad (2)$$

where, f is the rock strength ratio according to the Protodyakonov (1930) scale [20]; η - is the fraction of the initial energy remaining in the detonation products at the moment of complete expansion of the blast cavity. During the development of the Protodyakonov scale, Protodyakonov (1930) [20] introduced the concept of rock strength. Unlike the commonly used concept of material strength, which is assessed based on a specific type of stress state (e.g., ultimate compressive strength, tensile strength, torsional strength, etc.), the rock strength parameter allows for comparing rock types based on the effort required for their destruction and extractability. He assumed that this parameter could be used to evaluate the combined effect of various stresses acting during rock failure, as occurs, for instance, in explosive fracturing.

$$\eta = \frac{\gamma_0 - 1}{k-1} \cdot \frac{373}{\gamma_{em}} \left(\frac{\sigma_{cs}}{P_0}\right)^{\frac{k-1}{k}} \quad (3)$$

where σ_{cs} – Uniaxial compressive strength of rocks, kg/m²; k – is the minimum value of the adiabatic index at a density of γ_{em} = 373 kg/m³, assumed to be 1.4; γ_{em}– explosive density, kg/m³. For the Rioflex OC 7000 explosive, at an explosive density of γ_{em}= 1200 kg/m³; P_0 – is the initial adiabatic index of expansion for high-density detonation products.

$$\gamma_0 = \sqrt{1 + \frac{\gamma_{em}^{1.2}}{1270}} \quad (4)$$

P_0 – is the initial pressure of the detonation products, kg/m², which can be expressed as:

$$P_o = (\gamma_0 - 1) \cdot \gamma_{em} \cdot U_{se} \quad (5)$$

where U_{se} – is the specific energy of the explosive, kg·m/kg, determined by the following formula:

$$U_{se} = 427 \cdot Q \quad (6)$$

where Q – is the specific heat of explosion, kcal/kg; 427 – mechanical equivalent of thermal energy, kg·m/kcal.

In the process of calculating of the seismicity ratio and determining the displacement velocity of the rock mass at a given distance, the input data included the mechanical properties of the rocks at the deposit and the specification of the explosives used in blasting operations at the open-pit mine. For ground vibration assessment were used vibrometers ZET7152N ver2. To assess the reducing the ground particles displacement velocity and acceleration were used 3 vibrometers at different distance from the blasting epicentre (Figure 2).

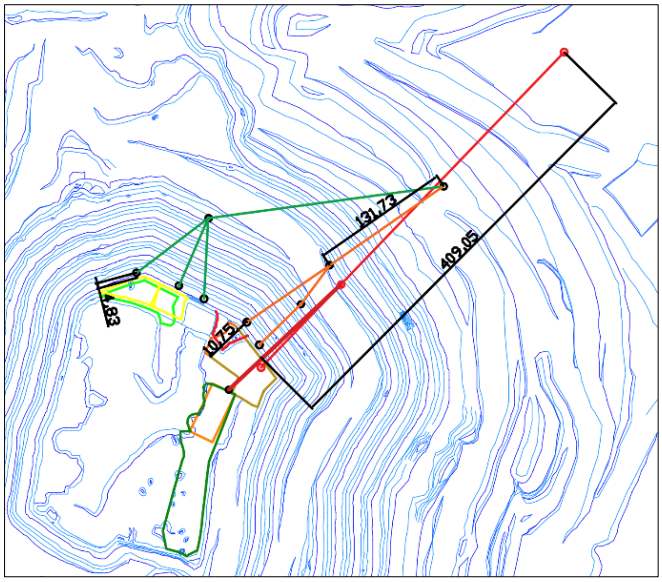

Figure 2. The placement scheme of the vibrometers

There were assessed rock fragmentation in WipFrag software after each blast. Also was assessed the slope stability. For the assessment slope stability were used tacheometers. Totally on the 9 experimental blocks were provided blasting with electronical initiating systems. The results were compared with the other blocks where were used nonelectrical initiating systems. There were used 2 types of the borehole spacing: 5×4.5 m and 3.5×3.5 m at experimental blocks. Each blasting was provided by ground vibration monitoring, fragmentation analysis and slope stability analysis.

For seismic monitoring, a system consisting of three ZET7152N ver2 vibrometers was used. The 3 vibrometers were positioned normal to the blasted blocks on the pit benches at distances ranging from 6 to 120 meters (Figure 2). For discovering PPV in the closest area from blasting, one of the three vibrometers was placed as close to blasted block as it was possible. The fragmentation analysis was based on a series of photographs taken with a camera (Figure 3).

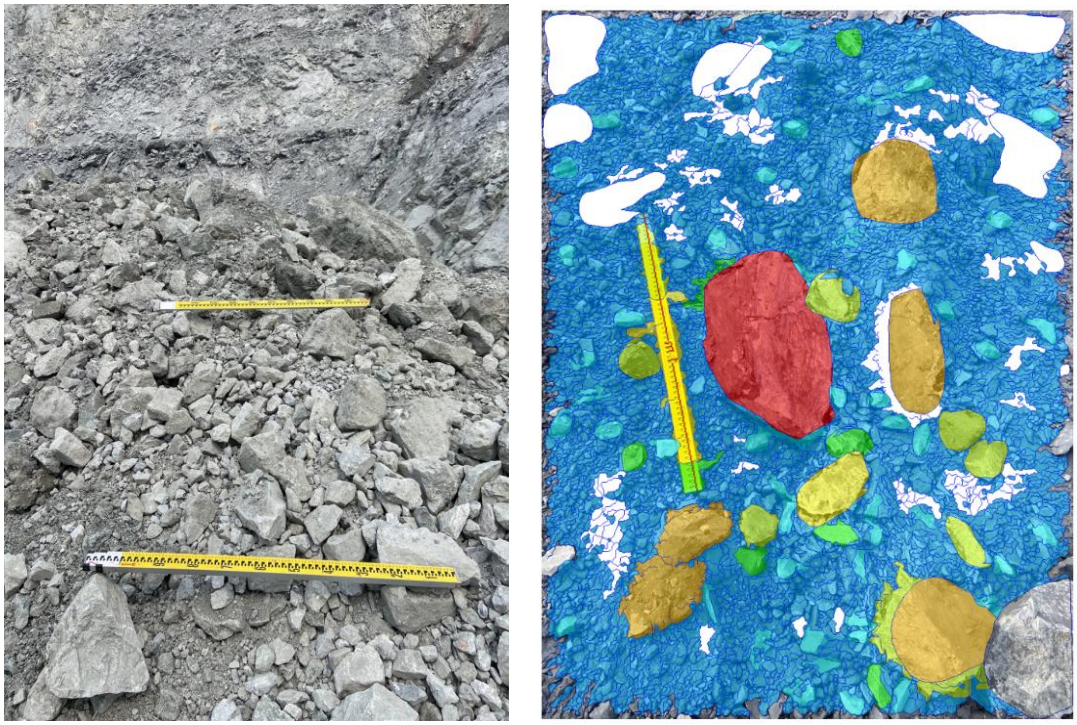

Figure 3. Sample photograph for fragmentation analysis

To monitor the displacement of pit walls and benches, eight control benchmarks were installed on the upper benches. The coordinates were measured using a Leica 1205+ total station. Initially, measurements were taken after the installation of the benchmarks on the benches. Subsequent measurements were conducted after each blast. A total of six surveys were carried out (Figures 4 and 5).

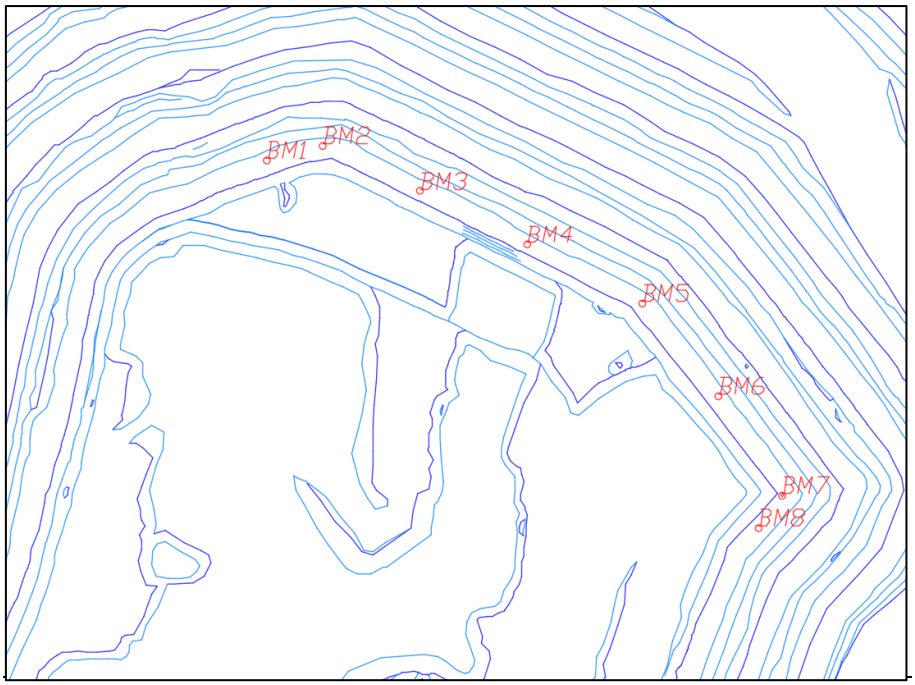

Figure 4. The placement scheme of the benchmarks

Figure 5. Example of the benchmark

3. Experiments/Research

Based on the experiments were point out the blocks with the most effective blast results and with registered minimal ground vibrations. Also, there were assessed the slope surfaces close to the blasted area before and after the blasts (Figure 4). There are 3 types of rocks at the discussed open pit mine. The properties of rocks shown in the Table 2. All of them have the same density 2.8 – 2.99 kg/m^3 (Table 2).

There were conducted nine experimental blasts during the experiment, including: 3 blasts using non-electric initiation systems (NEIS) and 6 blasts using electronic initiation systems (EIS). Rioflex explosive was used for blasting dry and waterlogged boreholes (Table 3). The blasting of boreholes was short-delayed, using the non-electric blasting system "Rionel" (Table 3). Depending on the geological conditions boreholes with diameters of 115 and 165 mm were used.

Table 2. Types of Rocks and Their Properties

Rock type	Fracturing degree	Density t/m³	Unit weight t/m³	Compressive strength MPa	Elastic modulus MPa	Tensile strength MPa	Poisson's ratio	Protodyakonov [20] strength ratio	Seismicity ratio by [19]
1	2	3	4	5	6	7	8	9	10
Basaltoids	Slightly Fractured	2.99 2.75-3.35	2.94 2.75-3.25	166.3 139.2-243.1	10.83 10.61-11.22	19.8 15.2-22.6	0.26 0.25-0.28	16.1 13.9-18.5	6.29
	Medium Fractured	2.94 2.72-3.01	2.71 2.69-2.82	121 115.2-138.3	8.17 6.01-10.12	12.1 7.7-16.2	0.29 0.28-0.30	15.2 11.7-16.5	8.22
	Severely Fractured	2.92 2.70-2.99	2.60 2.59-2.70	71.9 65.2-114.1	5.10 4.81-6.28	2.7 1.4-6.9	0.30 0.29-0.31	13.2 8.8-14.7	8.849
	Loose-Clastic	2.91 2.70-2.98	2.49 2.39-2.61	36.3 32.8-43.7	3.02 2.21-4.89	———	0.34 0.30-0.35	5.18 4.1-6.2	6.906
Diorite porphyrites	Slightly Fractured	2.92 2.77-3.01	2.89 2.73-2.99	122.8 95.8-135.1	9.73 8.76-10.06	15.1 12.1-16.0	0.25 0.24-0.26	15.8 11.5-17.7	8.314
	Medium Fractured	2.87 2.76-2.92	2.76 2.69-2.80	90.1 74.5-99.7	7.22 6.05-8.31	10.4 8.7-12.4	0.27 0.26-0.28	10.7 9.0-11.2	7.785
	Severely Fractured	2.83 2.76-2.90	2.57 2.56-2.64	75.5 69.9-83.2	5.02 4.61-7.99	5.2 3.5-6.8	0.30 0.28-0.31	8.2 6.2-9.7	7.268
	Loose-Clastic	2.79 2.75-2.90	2.51 2.40-2.61	24.4 20.2-30.5	2.30 1.71-4.30	———	0.34 0.30-0.35	5.1 4.4-6.4	6.906
Carbonate clay rocks (metasomatites; skarns; skarned rocks)	Slightly Fractured	2.98 2.79-3.62	2.95 2.76-3.60	193.1 178.5-212.8	11.8 9.81-12.83	15.9 13.5-17.8	0.24 0.23-0.25	16.3 14.0-17.7	6.292
	Medium Fractured	2.95 2.79-2.99	2.82 2.67-3.81	151.1 102.0-180.1	8.47 6.23-10.04	10.9 8.7-12.1	0.27 0.25-0.28	12.3 9.8-14.4	6.876
	Severely Fractured	2.86 2.76-2.90	2.50 2.40-2.57	80.9 43.6-107.4	5.62 4.11-6.47	4.7 3.3-8.9	0.30 0.27-0.31	9.1 7.6-10.2	7.471
	Loose-Clastic	2.80 2.70-2.86	2.31 2.14-2.41	21.1 16.2-44.1	2.01 1.02-4.40	———	0.35 0.34-0.35	6.0 4.4-8.0	8.551

Table 3. Explosives specifications

№	Type	Anfo	Water resistance	Average in hole Density (g/cm³)	Velocity of Detonation, m/s
1	Rioflex 7000	30%	Excellent	1.00-1.28	3500-7200
2	Rioflex 10000	0%	Excellent	1.00-1.35	3700-7350

The details of the blasts are provided in Table 4.

Table 4. Blasting specifications on experimental blocks

№	Block name	Volume, m³	Burden and Spacing, m	Delay	Initiation system
1	90-027	14269	5×4.5	25, 17 ms	NIES
2	90-027-2	7000	5×4.5	25, 17 ms	NIES
3	90-066	3252	5×4.5	25, 17 ms	NIES
4	95-066	3176	5×4.5	25 ms/m	EIS
5	95-068	4238	5×4.5	20 ms/m	EIS
6	95-026	7872	5×4.5	30 ms/m	EIS
7	90-026-2	3424	3.5×3.5	25 ms/m	EIS
8	90-028	3452	3.5×3.5	36 ms/m	EIS
9	90-029	2746	3.5×3.5	20 ms/m	EIS

Table 4 presents the blasting burden and spacing parameters for each blasted block. In addition, it includes the volume of blasted rock mass, the initiation system used, and the inter-hole delay intervals.

4. Results

As a result of a series of experimental blasts, valuable data on PPV at various distances ranging from 6.5 to 451 meters were obtained (Table 5). After each blast, benchmark measurements were conducted to monitor potential displacements (Table 6). A fragmentation analysis was performed for each blasted block and the results shown in Table 7.

Table 5. Peak values of vibration velocity

№	Block name	Sensor number and distance from the blasted block	X-axis PPV (mm/s)	Y-axis PPV (mm/s)	Block volume (m^3)	Number of boreholes
1	90_027	1-st, 35.69 m	18.72	40.31	14269	160
		2-nd, 160 m	7.16	5.19		
		3-rd, 451 m	0.8	1.58		
2	90_027_2	1-st, 13.71 m	192.77	510.24	7000	70
		2-nd, 71.39 m	5.76	8.25		
		3-rd, 225.31 m	2.54	3.21		
3	90_066	1-st, 10.72 m	29.38	36.81	3252	31
		2-nd, 106.26 m	3.43	3.42		
		3-rd, 237.99 m	0.95	0.78		
4	95_067	1-st, 6.57 m	138.83	83.37	3176	35
		2-nd, 14.93 m	33.42	24.46		
		3-rd, 78.32 m	9.34	12		
5	95_068	1-st, 8.21 m	49.89	58.53	4238	42
		2-nd, 33.02 m	28.5	23.38		
		3-rd, 81.88 m	17.14	19.16		
6	90_026	1-st, 10.71 m	159.56	81.98	7872	81
		2-nd, 65.63 m	27.7	15.17		
		3-rd, 110.7 m	3.65	4.14		
7	90_026_2	1-st, 13.1 m	11.48	15.73	3424	52
		2-nd, 74.84 m	17.69	4.49		
		3-rd, 118.83 m	0.97	1.55		
8	90_028	1-st, 25 m	10.21	8.55	3452	62
		2-nd, 60.93 m	7.94	5.24		
		3-rd, 80.41 m	3.62	11.95		
9	90_029	1-st, 14.94 m	47.33	19.19	2746	44
		2-nd, 63.98 m	4.43	4.18		
		3-rd, 95.3 m	2.2	3.87		

Table 6. Results of monitoring slope displacements caused by blasting

Measure №	Benchmarks	ΔX, m	ΔY, m	ΔZ, m
1	BM1	-0.015167	0.00897	0.0147
	BM2	0.003933	0.01943	0.01566667
	BM3	0,0033	0.00633	0.00863333
	BM4	-0.009367	0.01453	0.02753333
	BM5	-0.0047	0.00863	0.01786667
	BM6	0.000233	0.0007	0.0058
	BM7	-0.003667	0.0079	0.00473333
	BM8	0.0006	0.0035	0.0018
2	BM1	0.005167	-0.02374	0.0077
	BM2	0.0103	-0.02076	0.00466666
	BM3	0.0166	-0.01625	0.00158334
	BM4	0.0055	-0.0283	0.0003
	BM5	0.005167	-0.0225	0.00183333
	BM6	0.002367	-0.01777	0.00613333
	BM7	-0.0265	0.0051	0.0005
	BM8	-0.009667	-0.0136	0.01236667

3	BM1	0.015167	-0.00897	-0.0147
	BM2	-0.003933	-0.01943	-0.01566667
	BM3	0.0101	0.00515	0.00335
	BM4	0.0168	0.00687	0.01053334
	BM5	-0.0146	0.01194	0.03486667
	BM6	-0.000233	-0.0007	-0.0058
	BM7	0.0195	-0.0173	0.00373334
	BM8	-0.007966	0.00917	0.0347
4	BM1	-	-	-
	BM2	-0.002633	0.01979	0.02166667
	BM3	-0.0132	0.00627	0.01116666
	BM4	-0.005933	0.01167	0.00306666
	BM5	0.019433	0.00413	-0.02796667
	BM6	0.002566	0.013	0.0052
	BM7	0.005634	0.00683	0.01166666
	BM8	0.0241	-0.00624	-0.01216667
5	BM1	-	-	-
	BM2	-	-	-
	BM3	0.014067	-0.00627	-0.01036666
	BM4	0.057733	-0.0077	0.01343334
	BM5	0.050167	0.00563	0.00016667
	BM6	-0.0107	0.0045	-0.00616666
	BM7	-0.0021	-0.0052	-0.0043
	BM8	-0.0023	-0.0081	-0.0121
6	BM1	-	-	-
	BM2	-	-	-
	BM3	-0.027367	0.00747	-0.0013
	BM4	-0.066233	0.00413	-0.01766667
	BM5	-0.056167	-0.00913	0.00846666
	BM6	0.006834	-0.0083	0.01456666
	BM7	0.015933	0.0036	-0.0081
	BM8	0.0009	-0.00116	6.667E-05

As shown in the table registered PPV value varies from 0,8 to 510 mm/s. The highest peak particle velocity (PPV) among all blocks blasted using EIS was measured during the blasting of block 95_026, attaining 159.56 mm/s at a distance of 10.71 meters, with a borehole spacing of 5 × 4.5 meters and a delay interval of 30 ms/m. Under NEIS conditions, the maximum PPV was recorded during the blasting of block 90_027_2, reaching 510.24 mm/s at a distance of 13.71 meters.

$$PPV = K \cdot \left(\frac{R}{\sqrt{Q_{max}}}\right)^{-b} \quad (7)$$

According to the Equation 1 [21], scaled distance (SD) values were used for comparing blast results. The maximum weight of a single charge series is presented in Table 8. As shown in Table 8, the blocks were grouped based on the initiation system used and the average charge per blast. The last group of EIS blocks (90_026_2, 90_028, 90_029), due to changes in blast hole grid parameters and a significant data spread associated with geological conditions, exhibited a low correlation level. Consequently, these blocks are not suitable for comparison with NEIS under this criterion.

Table 7. Fragmentation Analysis of Blasted Blocks

Block name	90-027	90-027-2	95-066	95-067	95-068	95-026	90-026-2	90-028	90-029
Type of initiation system	NEIS	NEIS	NEIS	EIS	EIS	EIS	EIS	EIS	EIS
Step size	0.05	0.05	0.05	0.05	0.05	0.05	0.05	0.05	0.05
Minimum range	0.05	0.05	0.05	0.05	0.05	0.05	0.05	0.05	0.05
Maximum range	3	3	3	3	3	3	3	3	3
Sample size	47781	13849	9639	186787	24070	23829	29242	79279	72958
Minimum value in the sample	0.001	0.001	0.001	0.001	0.001	0.001	0.001	0.001	0.001
Maximum value in the sample	3.8983	5.3655	3.7464	2135.5631	12.1963	4.5116	4.3632	3.1433	3.6332
Arithmetic mean	0.4104	0.2968	0.554	0.2304	0.6054	0.4734	0.3452	0.3894	0.4357
Mode	0.075	0.075	0.075	0.0750	0.0750	0.0750	0.0750	0.0750	0.0750
Median of the statistical series	0.225	0.175	0.325	0.1250	0.3750	0.3250	0.2250	0.2250	0.2750
Mathematical expectation	0.4117	0.298	0.5547	0.2329	0.6062	0.4741	0.3461	0.3904	0.4364
Variance	0.2133	0.1252	0.2996	0.0892	0.3725	0.2300	0.1146	0.1602	0.1884
Standard deviation	0.4619	0.3538	0.5473	0.2987	0.6104	0.4796	0.3385	0.4003	0.4341
Coefficient of variation	1.1218	1.1872	0.9867	1.2823	1.0068	1.0116	0.9779	1.0252	0.9946
Skewness	2.2854	3.2836	1.6841	4.2670	1.6326	2.1093	2.6422	2.2033	2.1420
Kurtosis	6.0325	13.9382	2.8021	23.9028	2.2532	5.0572	10.53	5.8092	5.3840
Average fragment size. m	**0.4367**	**0.3230**	**0.5797**	**0.2579**	**0.6312**	**0.4991**	**0.3711**	**0.4154**	**0.4614**
Percentage of oversize fraction	49.32	41.18	60.18	55.16	71.17	53.36	28.54	40.98	42.97
Blast hole pattern. m	5×4.5	5×4.5	5×4.5	5×4.5	5×4.5	5×4.5	3.5×3.5	3.5×3.5	3.5×3.5
Delay time. ms	25	25	25	25	20	30	25	36	20
Number of blast holes. pcs	160	70	31	35	42	81	52	62	44
Rock mass volume. m^3	14269	7000	3252	3176	4238	7872	3424	3452	2746
Explosive weight. kg	11413	5098	2205	2510	3184	6378	2445	2784	2114
Powder factor of EM. kg/m^3	0.8	0.73	0.68	0.79	0.75	0.81	0.71	0.81	0.77
Average charge per blast hole. kg	71.33	72.83	71.13	71.71	75.81	78.74	47.02	44.9	48.05

Table 8. Site constants for NIES and EIS blasted group of blocks

№	Initiation system	Block name	Average charge per blast hole, kg	Site constants	
				X_{axis}	Y_{axis}
1	NEIS Group 1	90_027	71.33	b: 1.22	b: 1.36
		90_027_2	72.83	K: 107.1	K: 198.5
		95_066	71.13	R^2: 0.84	R^2: 0.795
2	EIS Group 2	95_067	71.71	b: 0.96	b: 0.81
		95_068	75.81	K: 92.9	K: 64.82
		95_026	78.74	R^2: 0.77	R^2: 0.82
3	EIS Group 3	90_026_2	47.02	b: 1.07	b: 0.79
		90_028	44.9	K: 53.3	K: 29.9
		90_029	48.05	R^2: 0.56	R^2: 0.66

The calculation of the coefficients K and b was performed using the linear regression (Table 9). When using NIES, based on the dataset from Table 5, a regression line was plotted using for the mentioned method (Figure 6). For EIS separated by the two groups (Table 8) data shown at Figures 7 and 8.

Table 9. Site constants for NIES and EIS blasted group of blocks

№	Initiation system	Block name	Average charge per blast hole, kg	Site constants (R^2=1)	
				b	K
1	NEIS Group 1	90_027	71.33	1.499	7.89
		90_027_2	72.83		
		95_066	71.13		
2	EIS Group 2	95_067	71.71	1.5	7.88
		95_068	75.81		
		95_026	78.74		
3	EIS Group 3	90_026_2	47.02	1.5	7.99
		90_028	44.9		
		90_029	48.05		

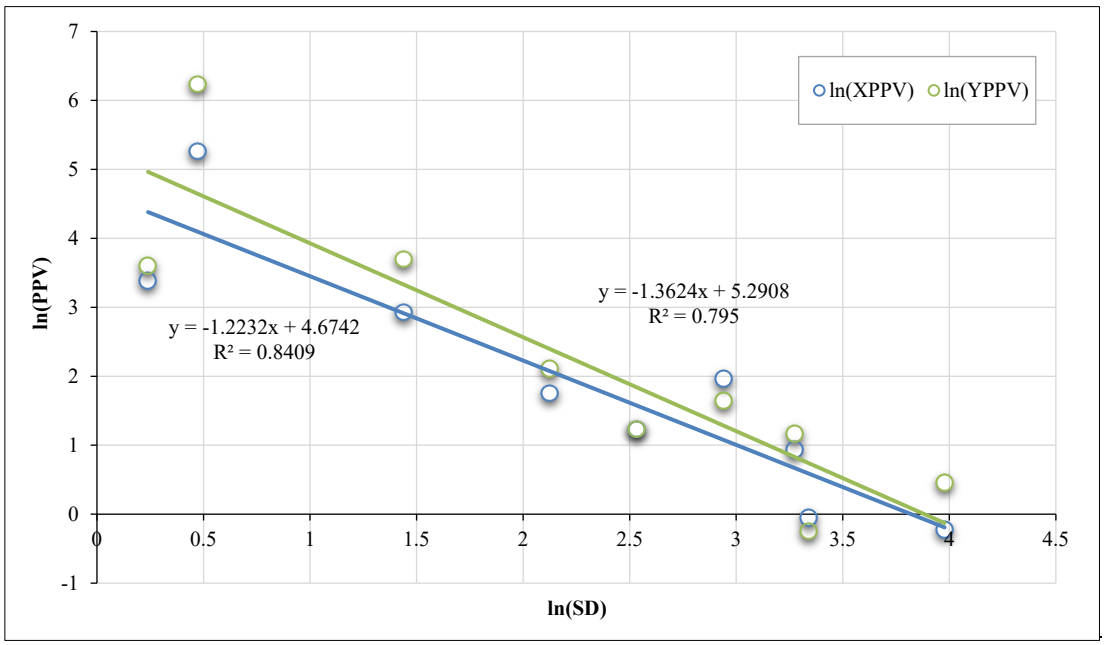

Figure 6. Vibration attenuation chart using NIES for first group

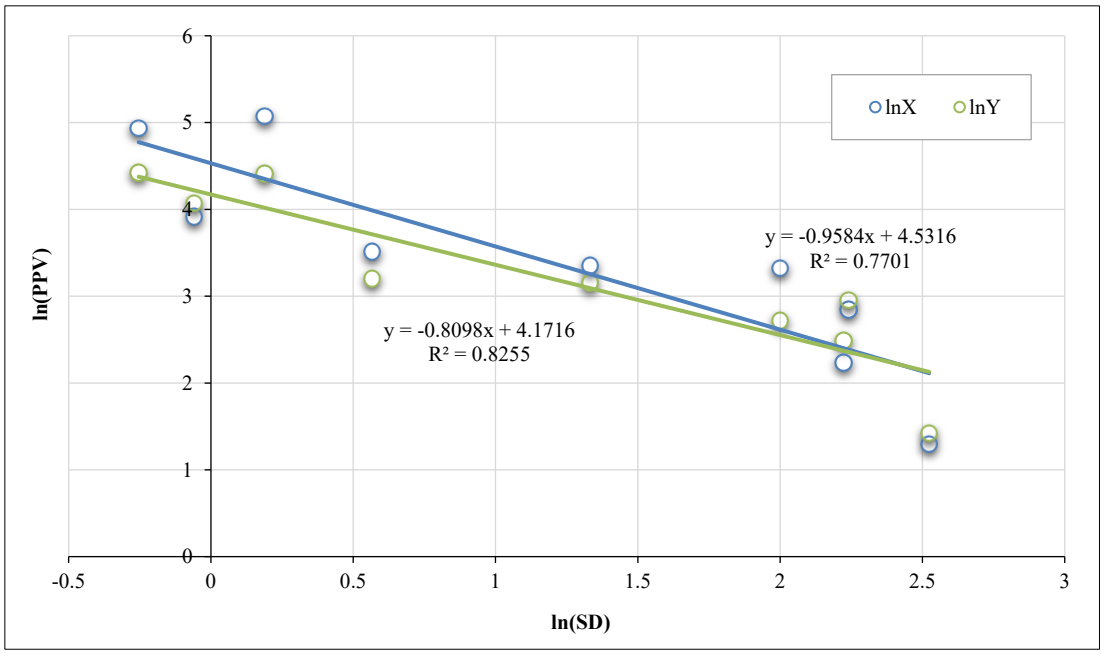

Figure 7. Vibration attenuation chart using EIS for second group

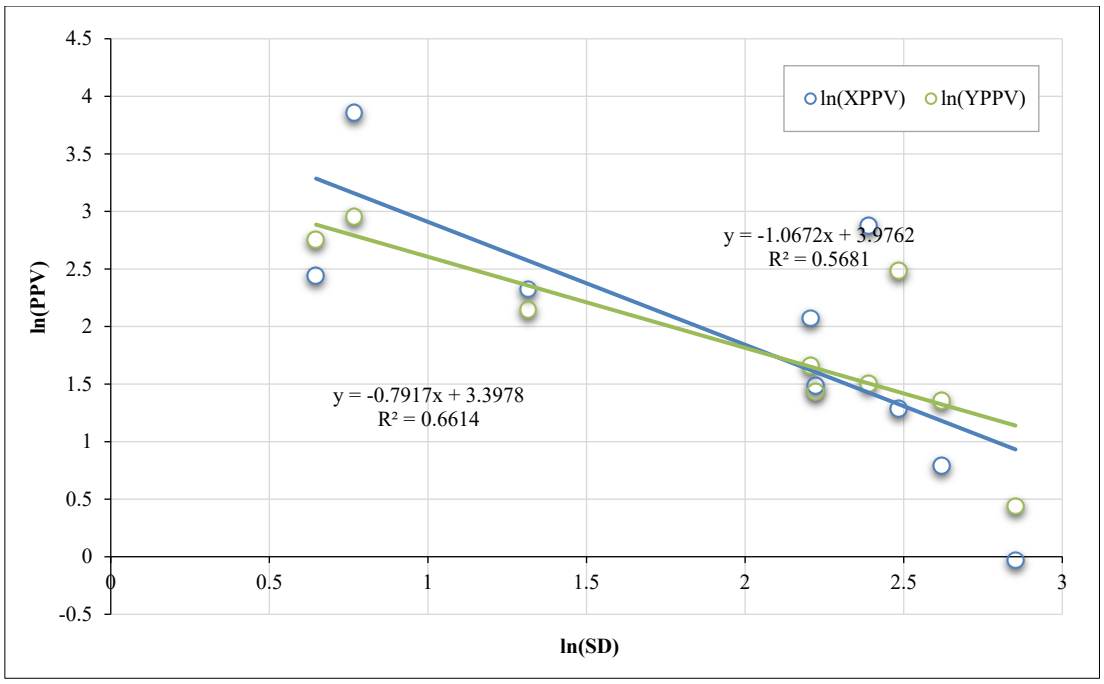

Figure 8. Vibration attenuation chart using EIS for third group

On the other hand, Group 1 (Figure 9) demonstrates a higher attenuation coefficient compared to Group 2 (Figure 10). Moreover, the K coefficient values for Group 1 exceed those of Group 2 by 113%. From this, it can be inferred that the blast waves of the first group are characterized by higher initial vibration and faster attenuation, whereas the second group exhibits lower amplitude but vibration propagates over a greater distance.

The fragmentation analysis of the blasted rock mass was conducted by WipFrag and K-mine software. As acceptable size of the rocks defined 500 mm. Rock particles with size more than 500 mm were defined as oversized. Based on the data from Table 6, the following conclusions can be drawn:

There were less than 9.29% of oversized particles in first group of blasts using NEIS. The average rock particles size in first group of blasts were less than second group, where were used EIS, for 4.5%. It shows that reduction the vibration lead to losing the quality of blasts despite of using EIS.

However, when the blast hole grid parameters for EIS in third group (Figure 11) were changed from 5×4.5 m to 3.5×3.5 m while maintaining the specific explosive consumption, the following results were observed: compared to the NEIS blocks, the EIS block exhibited 12.73% less oversized particles and 6.8% smaller average size of particles. Therefore the blast quality depends mostly not only on the initiating technique but also on the blast hole grid.

The results of a series of slope displacements instrumental monitoring are presented in Table 6. There were installed eight benchmarks (BM1, BM2, … BM8) on the slope near the experimental area. The measurements were taken after each blast. Table 8 presents the results of the first geodetic survey (Measure № 1), showing the coordinate differences (ΔX, ΔY, ΔZ) for Benchmarks 1–8 measured before and after each blast. After the third blast BM1 was destroyed. After the fourth blast benchmark BM2 was also destroyed.

The survey results indicate that there have been no significant displacements in the monitoring area. Different vectors of the benchmark displacements demonstrate that the measured data are within the measurement error range. This suggests that the blasts have only affected the area locally and the slope is generally stable.

Meanwhile, the displacement velocity of the rock mass according to Sadovsky's formula [19] is described by the Equation 8:

$$PPV = Kc \cdot \left(\frac{Q^{\frac{1}{3}}}{R}\right)^{1.5} \quad (8)$$

where k_c – seismicity ratio, Q – average charge per blast hole, kg, R – distance from blast epicenter, m.

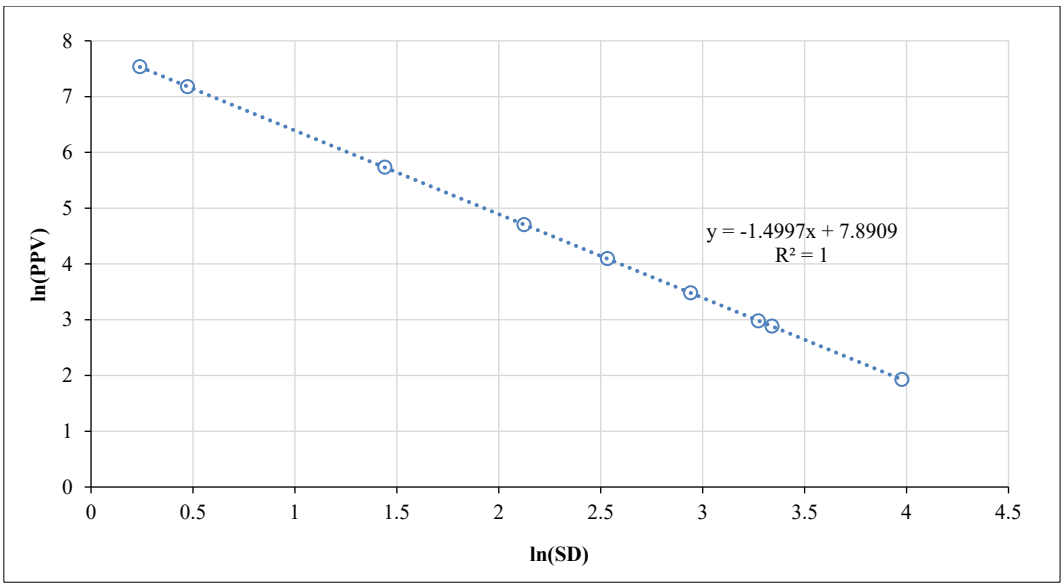

Figure 9. Vibration attenuation chart using NEIS for the first group

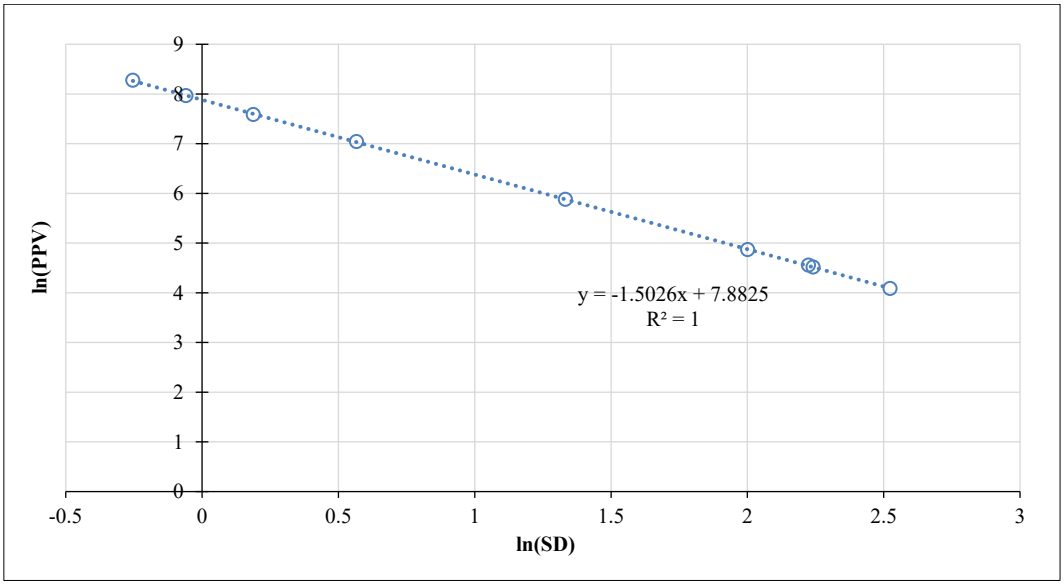

Figure 10. Vibration attenuation chart using EIS for the second group

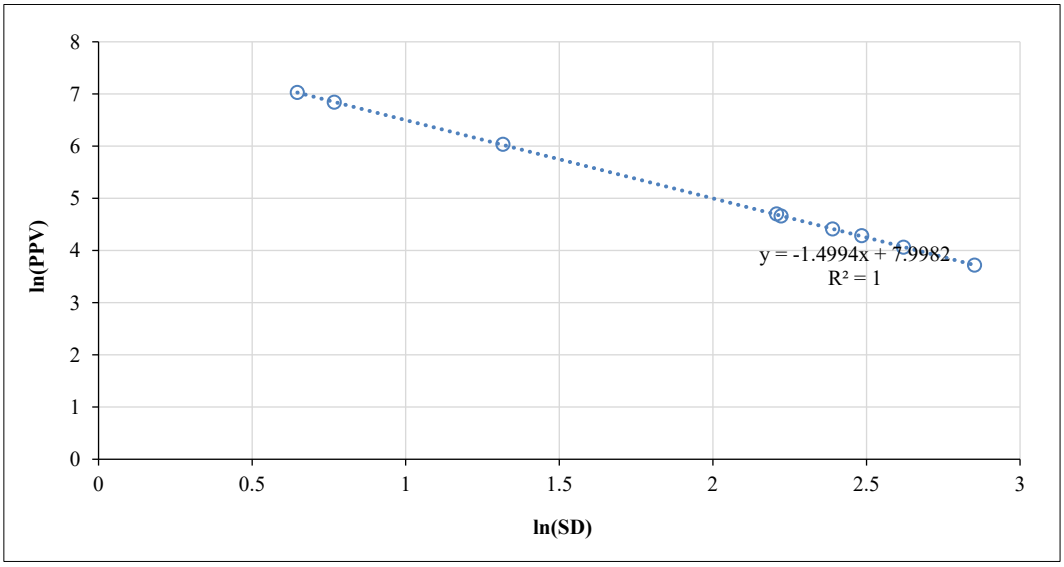

Figure 11. Vibration attenuation chart using EIS for the third group

The results of PPV calculations using Equations 7 and 8 were compared in this study. The comparison indicates a close agreement between the results obtained from both equations. Therefore, both Equations 7 and Equation 8 can be reliably used for predicting the expected PPV at specified distances from the blast source. However, the measured particle velocity values were lower than the theoretically calculated ones.

Such differences can be explained by the heterogeneity of the rock mass, the presence of structural weaknesses, and rock fracturing. For the discussed area there were calculated adjustment factors specifically for NEIS and EIS. Considering the applied correction factors for the case under study, the PPV equation based on Sadovsky's formulation (Equation 8) can be expressed in its adjusted form as Equation 9.

$$PPV = (Kc \times Kx) \cdot \left(\frac{Q^{\frac{1}{3}}}{R}\right)^{(1,5*bx)} \quad (9)$$

In this context, specific correction factors are assigned for each group, as presented in Table 10.

Table 10. Correction factors for NIES and EIS blasted group of blocks by Sadovsky equation

№	Initiation system	Block name	Average charge per blast hole, kg	Correction factors	
				X_{axis}	Y_{axis}
1	NEIS Group 1	90_027	71.33	bx: 0.813 Kx: 13.57	bx: 0.906 Kx: 25.15
		90_027_2	72.83		
		95_066	71.13		
2	EIS Group 2	95_067	71.71	bx: 0.64 Kx: 11.789	bx: 0.54 Kx: 8.225
		95_068	75.81		
		95_026	78.74		
3	EIS Group 3	90_026_2	47.02	bx: 0,713 Kx: 6.67	bx: 0.526 Kx: 3.74
		90_028	44.9		
		90_029	48.05		

5. Conclusions

In this study, we compared the efficiency and seismic impact of blasting operations using two initiation systems: electronic initiation systems and non-electric initiation systems. An analysis of the fragmentation of blasted rock mass was conducted.

During the research vibrometers were placed in various distances from the blast source. The closest distance of vibrometers placement from the blast source was 6 meters. It is much closer than vibrometer placement comparing with previous researches. Such close placement allows to study blast affection to the closest area. According to the Hoek and Brown the damage area can be extended up to 15 meter or slope height [22]. Survey shows that the measured values of PPV reached 510 mm/s at distance less than 10 meters. Observations demonstrated that, despite these displacement velocities, no significant structural changes in the rock mass were observed, thereby confirming the findings of earlier studies. Moreover, the measured displacements suggest that the use of EIS contributes to a reduction in the seismic effect on the rock mass. These findings confirm the potential of EIS as a controlled blasting method suitable for areas where conventional technologies cannot be applied.

In the countries of the former Soviet Union, the expected PPV is commonly estimated using the formula developed by Sadovsky. A comparison between Sadovsky's equation [19] and the empirical PPV prediction model described in Hossain Khan et al. [21] demonstrates their equivalence. The application of both formulas requires using correction factors for discussed area conditions. These adjusted equations provide a reliable basis for predicting PPV for the planning of blasts effects within the study area.

With relatively equal average fragmentation values, the PPV attenuation coefficient was higher when using non-electric initiation systems. However, when the blast hole pattern parameters were adjusted while using electronic initiation systems, the percentage of oversized fragments, the average fragment size, and the seismic impact—at a relatively equal specific explosive consumption—showed lower values. This demonstrates the effectiveness of EIS in scenarios where it is necessary to control seismic impact while maintaining fragmentation quality.

Therefore, in cases where other wall control blasting technology (presplit blasting, buffer blasting etc.) cannot be applied, electronic initiation systems can be used as alternative solution.

6. Declarations

6.1. Author Contributions

Conceptualization, B.N.B. and B.A.S.; methodology, A.O.A.; software, A.O.A.; validation, B.N.B.; formal analysis, A.O.A.; investigation, A.O.A.; resources, B.N.B.; data curation, A.O.A.; writing—original draft preparation, A.O.A.; writing—review and editing, A.O.A.; visualization, A.O.A.; supervision, B.N.B.; project administration, B.N.B.; funding acquisition, B.N.B. All authors have read and agreed to the published version of the manuscript.

6.2. Data Availability Statement

The data presented in this study are available on request from the corresponding author.

6.3. Funding

This study was financially supported by JSC Varvarinskoye under the Contract for Research and Development Work AOV 2(01-1-0467) dated October 20, 2020, and the Contract for Research and Development Work AOV 2(04-1-0040) dated April 12, 2023, which provided funding for the implementation of this research and the publication of this article.

6.4. Conflicts of Interest

The authors declare no conflict of interest.

7. References

[1] Appani, R., Harsha, V., & Subrahmanyam, S. K. (2025). Development of an equation to predict blast induced ground vibrations of open cast lime stone mine by using Multiple Linear Regression (MLR). Disaster Advances, 18(5), 30–36. doi:10.25303/185da30036.

[2] Aruna, M., Vardhan, H., Tripathi, A. K., Parida, S., Raja Sekhar Reddy, N. V., Sivalingam, K. M., Yingqiu, L., & Elumalai, P. V. (2025). Enhancing safety in surface mine blasting operations with IoT based ground vibration monitoring and prediction system integrated with machine learning. Scientific Reports, 15(1), 3999. doi:10.1038/s41598-025-86827-w.

[3] Leng, Z., Fan, Y., Lu, W., Gao, Q., & Yang, G. (2025). Failure mechanisms of electronic detonators subjected to high impact loading in rock drilling and blasting. International Journal of Coal Science and Technology, 12(1), 10. doi:10.1007/s40789-025-00749-6.

[4] Hong, Z., Tao, M., Feng, S., Liu, H., Wu, W., Li, X., & Liu, S. (2025). Experimental study of the impact of deck-charge structure on blast-induced fragmentation. Geomechanics and Geophysics for Geo-Energy and Geo-Resources, 11(1), 3. doi:10.1007/s40948-024-00915-1.

[5] Tosun, A. (2022). A new method for determining muckpile fragmentation formed by blasting. Journal of the Southern African Institute of Mining and Metallurgy, 122(11), 665–672. doi:10.17159/2411-9717/1104/2022.

[6] Li, T., Song, L., Chen, M., Guo, B. W., Fan, B., & Cui, S. S. (2025). Analysis of the characteristics of blasting seismic wave induced by explosive blasting with different coupling medium. Scientific Reports, 15(1), 6721. doi:10.1038/s41598-025-86682-9.

[7] Shehu, S. A., & Hashim, M. H. M. (2021). Evaluation of blast efficiency in aggregate quarries: facts and fictions. Arabian Journal of Geosciences, 14(6), 502. doi:10.1007/s12517-021-06526-4.

[8] Deressa, G. W., Choudhary, B. S., & Jilo, N. Z. (2025). Optimizing blast design and bench geometry for stability and productivity in open pit limestone mines using experimental and numerical approaches. Scientific Reports, 15(1), 5796. doi:10.1038/s41598-025-90242-6.

[9] Eremenko, A. A., & Filippov, V. N. (2020). Determination of Rational Drilling and Blasting Parameters To Ensure Stability of Edges of Open-Pit Mines in the Bystrinsky Deposit. Fundamental and Practical Questions of Mining Sciences, 7(1), 64–73. doi:10.15372/fpvgn2020070110.

[10] Bauer, A., & Calder, P. N. (1970). Open pit and blasting. Seminar Mining Engineering Department Publication, Queen's University, Kingston, Canada.

[11] Oriard, L. L. (1982). Blasting effects and their control. Underground Mining Methods Handbook, 378, 1590-1603.

[12] Holmberg, R., & Persson, P. A. (1978). Swedish Approach To Contour Blasting. Proceedings of Fourth Conference on Explosive and Blasting Techniques, 113–126.

[13] Rustan, A., Naarttijaervi, T., & Ludvig, B. (1985). Controlled Blasting in Hard Intense Jointed Rock in Tunnels. CIM Bulletin, 78(884), 63–68. doi:10.1016/0148-9062(86)90204-4.

[14] Meyer, T., & Dunn, P. G. (1996). Fragmentation and rock mass damage assessment: Sunburst excavator and drill and blast. Rock mechanics tools and techniques, 19-21 June, 1996, Montréal, Canada.

[15] Murthy, V. M. S. R., Dey, K., & Raitani, R. (2003). Prediction of overbreak in underground tunnel blasting: A case study. Journal of Canadian Tunneling Canadien, Toronto, Canada

[16] Dey, K. (2004). Investigation of blast-induced rock damage and development of predictive models in horizontal drivages. Ph.D. Thesis, Indian School of Mines Dhanbad. India.

[17] Arora, S., & Dey, K. (2010). Estimation of near-field peak particle velocity: A mathematical model. Journal of Geology and Mining Research, 2(4), 68-73.

[18] Bogdanoff, I. (2020). Vibration measurements in the damage zone in tunnel blasting. In Rock Fragmentation by Blasting. CRC Press, boca Raton, United States. doi:10.1201/9781003078104-24.

[19] Sadovsky, M. A., & Kostyuchenko, V. N. (1988). On the attenuation of seismic waves of an explosion in a rock mass. Reports of the Academy of Sciences, 30(6). (In Russian).

[20] Protodyakonov, M. M. (1930). Rock pressure and mine support. Part 1: Rock Pressure, 688E7D9B. (In Russian).

[21] Hossain Khan, M. F., Hossain, M. J., Ahmed, M. T., Monir, M. U., Rahman, M. A., Sweety, T. S., Akash, F. A., & Shovon, S. M. (2025). Ground vibration effect evaluation due to blasting operations. Heliyon, 11(2), 41759. doi:10.1016/j.heliyon.2025.e41759.

[22] Hoek, E., & Brown, E. T. (2019). The Hoek–Brown failure criterion and GSI – 2018 edition. Journal of Rock Mechanics and Geotechnical Engineering, 11(3), 445–463. doi:10.1016/j.jrmge.2018.08.001.